Impact of model resolution on the sea level simulation of the north Indian Ocean

Teesha Mathew[1,2], Abhisek Chatterjee[1,*], Lakshmi R Shenoy[1,2] and Satya Prakash[1]

1. Indian National Centre for Ocean Information Services (INCOIS), Ministry of Earth Sciences, Hyderabad, India

2. Kerala University of Fisheries and Ocean Studies (KUFOS), Kochi, Kerala, India

*Corresponding Author: Abhisek Chatterjee, Email: abhisek.c@incois.gov.in

Abstract

High resolution eddy resolving models are shown to be necessary for simulating submesoscale variability of the ocean. Although how these resolved submesoscale features impact the larger scale simulations is not yet clear. Here, using satellite observation and model experiments based on Modular Ocean Model (MOM5), we investigate the impact of model resolution in the sea level variability of the north Indian Ocean in the seasonal and intraseasonal time scale. While one model experiment uses uniform 0.25^{o} horizontal resolution with 40 vertical levels, in the second experiment model resolution is increase to uniform 0.05^{o} in horizontal with 50 vertical levels. The high resolution model shows significant improvement in simulating mean sea level and its variability especially along the coast of India, in the equatorial regime and in the western Arabian Sea. The Great Whirl and its extension become more realistic as the resolution increases. We show that these improvements are owing to the better representation of the mesoscale variability of the upper ocean water column. Further, we show that the coarser model tends to get biased towards wind-driven Ekman circulation in the open ocean and produce stronger seasonal signal along the coast.

Keywords: Ocean modeling, horizontal resolution, vertical levels, mesoscale variability, eddy kinetic energy.

1. Introduction

The north Indian Ocean is a tropical basin and is bounded by the continental boundaries of Arabia and Africa in the west, south Asia (India) in the north and south-east Asia in the east. In the east, it is connected to the Pacific Ocean via the Indonesian archipelago and in the south, it is open to the Southern Ocean. The Indian Peninsula divides the north Indian Ocean into two parts: the salty Arabian Sea (AS) in the west and the fresher Bay of Bengal (BoB) in the east (Figure 1). Despite being in a similar latitude belt, BoB and the AS exhibits strong contrast in the sea level, stratification and current systems. Further, it is driven by the seasonally reversing monsoon winds to exhibits a large spectrum of spatial and temporal scales. These scale-to-scale interactions to cascade energy from one spectrum to the other and its feedback to the atmosphere, particularly to the Indian monsoon, provides a challenge to the ocean modelling framework (McCraery et al., 1993; Schott and McCreary, 2001, Shankar et al., 2002; Schott et al., 2009; Phillps et al., 2021). There is a growing interest to resolve a larger spectrum of spatial and temporal scales to represent surface/subsurface physical processes accurately. This approach thus necessitates an increase of model resolution which can resolve more small scale features and the inverse energy cascade to the mean seasonal variabilities. Given the fact that the Indian Ocean is a tropical basin, the first baroclinic Rossby radius of deformations is in the order of ~50 km or more. Considering that a minimum of two grid points is required to resolve the first baroclinic mode (Hallberg, 2013), models with a horizontal resolution of ~1/4^{o} (or ~ 25 km) can resolve the first mode in most parts of the basin and thus, considered to be “eddy permitting” for the Indian Ocean. These models are shown to be able to reproduce seasonal variability of the Indian Ocean quite well (Kurian and Vinayachandran, 2006; Chatterjee et al., 2013; Shankar et al., 2016; Prerna et al., 2019; Chatterjee et al., 2019; Lakshmi et al., 2020). However, as the Rossby radius of deformation decreases rapidly close to the coast over the shelf or due to progressive change in the near-surface stratification, 1/4^{o} may fail to resolve the first mode explicitly. Further, it has

been shown that coastal currents along the east coast of India (East India Coastal Current; EICC) and along the west coast of India (West India Coastal Current; WICC) are strongly driven by higher order modes of much smaller length scale (Amol et al., 2012; Mukherjee et al., 2018; Francis et al., 2020a; Chaudhuri et al., 2020; Mukhopadhyay et al., 2020; Paul et al., 2021) and thus, the performance of these models of similar coarser resolution expected to fare poorly in these regions where such sub-mesoscale variabilities of length scale 10-50 km dominates. These models are therefore unable to resolve oceanic transient mesoscale features in the vicinity of the strong current regime or close to the boundary currents (Mukherjee et al., 2018; Francis et al., 2020b). As the resolution of the model increases sufficiently they explicitly resolve the Rossby radius of deformation for the first few baroclinic modes and are frequently referred to as "eddy resolving" models. To capture the interactions between the various physical and dynamical processes an increase in the resolution of numerical models is required (Hurrell et al. 2009; Shukla et al. 2009; Brunet et al. 2010). In the latitude belt of the central BoB or the AS, a resolution of ~$1/10^{o}$ is needed to resolve up to the first three vertical modes and ~$1/20^{o}$ is necessary to resolve up to the 10^{th} vertical mode (Shankar et al., 1996). These eddy resolving models tend to produce swift currents, jets and frontal systems as observed in the observations. While it is evident that eddy resolving models can produce realistic eddy structures and therefore, represent the associated frontal dynamics better over the coarser models, the impact of such improved representation of submesoscale features on the mesoscale simulation is still a subject of debate. A hierarchy of models is used in the past to assess the impact of horizontal resolution on the forced model simulation for the global ocean (Penduff et al., 2010; Griffies et al., 2015) and on a regional scale primarily for the northern Atlantic (Hurlburt and Hogan, 2000; Smith et al., 2000; Biri et al., 2016; Chassignet and Xu, 2017), for the coastal oceans around the Australian continent (Gou et al., 2020) and for the Pacific (Roberts et al., 2009; Lu et al., 2017). These studies indicate significant dynamical improvement in the representation of the boundary currents and associated eddy

activities. Nonetheless, in another study, Sandery and Sakov (2017) showed that high resolution submesoscale resolving model exhibit lower skill in forecasting mesoscale circulation compared coarser resolution eddy-resolving models. There are another set of studies where the impact of ocean model resolutions is investigated to understand air-sea feedback in the climate simulation (Roberts et al., 2004; Kirtman et al., 2012; Hewitt et al., 2017, 2020). Further, it has been also advocated that in line with the increased horizontal resolution, increasing vertical resolution is also necessary to improve horizontal (Stewart et al., 2017) and vertical processes (Ge et al., 2017; Jia et al., 2021) in the surface and subsurface water column.

Given the benefit shown by these high resolution models, operational centres across the globe are now moving towards high resolution models of resolution of the order of ~O(1) km scale. Unfortunately, the impact of model resolution in the simulation of the north Indian Ocean is still relatively unexplored. Hence, in this study, we seek to understand the impact of resolution on the simulated sea level variability and its spread in the frequency spectra for the north Indian Ocean. Here, we try to address the following questions: (1) How the increased resolution reflect onto the realism of the model simulation for the sea level? (2) What are the impact of model resolution on the open ocean and coastal sea level variability in seasonal and intraseasonal time scale and its mean state?

The rest of the paper is organized as follows: Section 2 describes the observations and model configurations used in this study. In Section-3 we discussed the impact of model resolution in the simulated sea level mean state and variability and discussed the primary results of this study. Finally, Section-4 summarizes the results.

2. Data

Here, we briefly describe the observations used in this study, the model configurations and experiment design.

2.1 Observations

Sea Level Anomaly (SLA) dataset based on delayed-time, merged multi-satellite, gridded product from AVISO (Archiving, Validation, and Interpolation of Satellite Oceanographic) is used in this study (www.aviso.oceanobs.com/fr/accueil/index.html ; Ducet et al., 2000). The daily data is available on a uniform 0.25° grid covering a period from 1993 onwards. Also, the global ocean surface current at 0.25° resolution from MOSDAC (http://www.mosdac.gov.in; Sikhakolli et al., 2013) is used for further analysis.

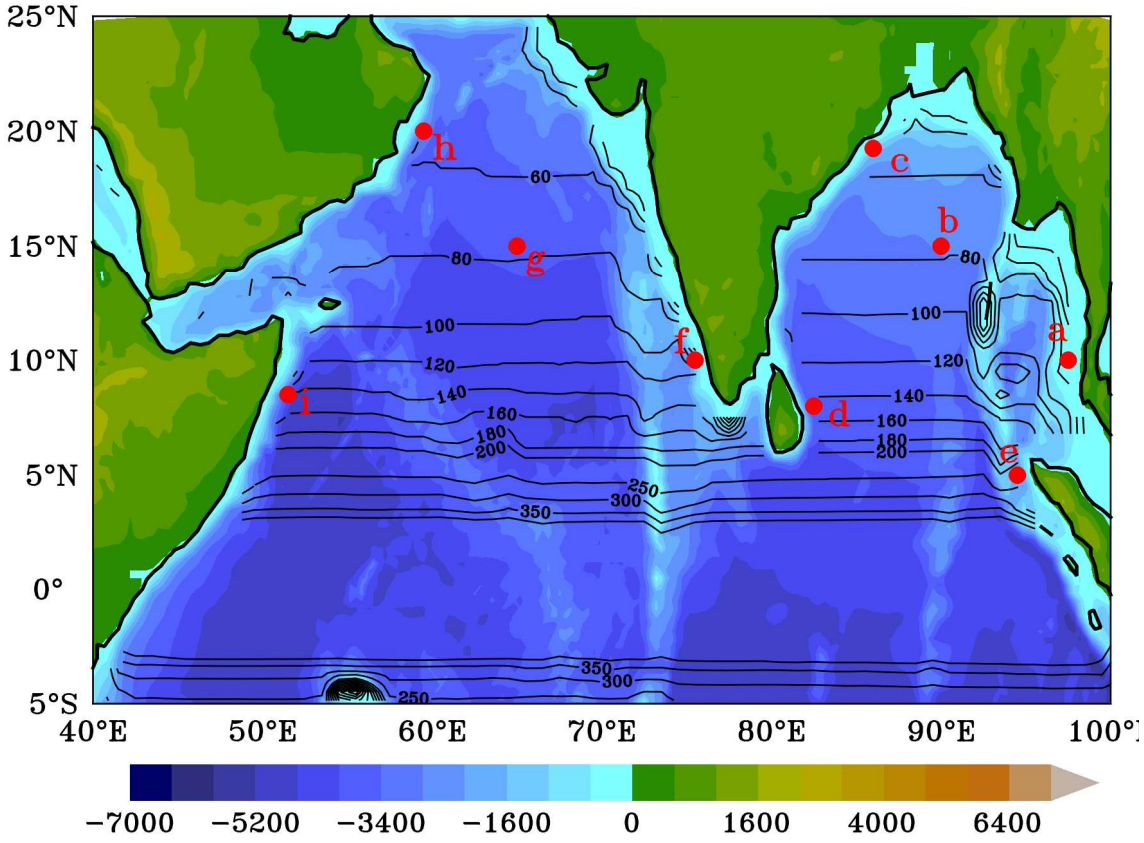

Figure 1: Bathymetry of the north Indian Ocean (shading) from Sindhu et al., (2007) and Rossby radius of deformation (kms) for the first baroclinic mode (contoured) calculated using climatological temperature and salinity from NIOA (Chatterjee et al., 2012). The red dots indicate the points used to compare MHMHR and MOMLR relative to altimeter SLA in later sections.

2.2 Model

In order to assess the impact of model resolution on the sea level simulation an ocean general circulation model based on Modular Ocean Model version 5 [MOM5, Griffies.,2012] is used in this study. The model uses hydrostatic, volume conserving, Boussinsque, primitive equations discretized on Arakawa B-grid with z-star vertical coordinate. The model domain

extends 30°S - 30°N and from 30°E - 120°E. The model's bottom topography is based on a modified ETOPO 5-minute gridded elevation dataset (Sindhu et al, 2007). At the land boundaries of the model domain, no-flux condition for tracers and no-slip and no-normal flow conditions for velocity fields are imposed. For temperature and salinity, 4° sponge layers based on NIOA (Chatterjee et al., 2012) are applied on the open southern and eastern boundaries with a restoration time-scale of 30 days. In this model vertical mixing follows the nonlocal K-profile parameterization (KPP) scheme based on Large et al., (1994). For horizontal diffusivity, a combination of Laplacian and biharmonic operator with a Smagorinsky-type mixing scheme is used.

2.2.1 Model Experiments

Two experiments are conducted in this study. In one experiment, horizontal resolution of the model was set to a coarser uniform 0.25° i.e. ~ 25 km. In the vertical, it uses 40 levels with 5 m resolution in the top 60 m and 18 levels in the upper 100 m of the water column. In this configuration, the minimum depth is set to 15 m (hereafter this experiment will be referred to as MOMLR). In another experiment, the horizontal resolution of the model is enhanced and set to uniform 1/20° i.e. ~5.5 km. Accordingly, vertical levels are also increased to 50 levels with 1-1.5 m resolution in the top 10 m and 24 levels in the top 100 m of the water column (Figure S1). Here, the minimum depth of a model grid is set to 5 m (hereafter this experiment will be referred to as MOMHR). For both the models, any cell shallower than the set minimum depth is deepened to maintain the minimum depth across the model domain.

Considering that the Rossby radius of deformation of the first baroclinic mode for the north Indian Ocean is 50 km or more (Figure 1), MOMLR can resolve the first mode in the entire domain except close to the coast or in the shelf seas. However, as the vertical mode increases the deformation radius decreases rapidly (Shankar et al., 1996) and therefore, MOMLR can no more resolve them explicitly. On the other hand, the MOMHR can resolve up to 10

vertical modes in the entire domain, thus can resolve the submesoscale variability more explicitly.

2.2.2 Forcing and model spin-up

Initially, the model is spun up for 25 years using daily climatological fields of momentum, radiative fluxes and windstress based on NCEP reanalysis product (Kalnay et al., 1996). Precipitation is taken from the Tropical Rainfall Measuring Mission (TRMM). Sea surface salinity is relaxed to NIOA (chatterjee et al., 2012) with a 15-day relaxation window. The model is initialised with temperature and salinity fields from NIOA climatology (Chatterjee et al., 2012) from a state of rest. The interannual simulation is carried for 7 years from 2011-2017 using the restart fields of the 35^{th} year of the climatological simulation. The interannual simulation model is forced by the 6 hourly atmospheric forcing at 0.25^{o} resolution based on Global Forecast System (GFS) obtained from National Centre for Medium Range Weather Forecasting (NCMRWF), Delhi. In the rest of the paper, results from this 7-year interannual simulation from both models are discussed.

3. Results

Here, we discuss the impact of model resolution on the mean seasonal cycle of SLA, and also on the variability at seasonal and mesoscale timescale. In order to understand the impact of model resolution on the simulated sea surface anomaly, first, we have re-gridded the high resolution model to the altimeter's 0.25^{o} grid so that both the model simulations can be compared with the observed SLA. Since, SLA for the altimeter is calculated from a geoid and for the model it is the deviation from the initial z = 0 level, the time-averaged mean of sea level is removed from the respective datasets to bring all of them in the same baseline.

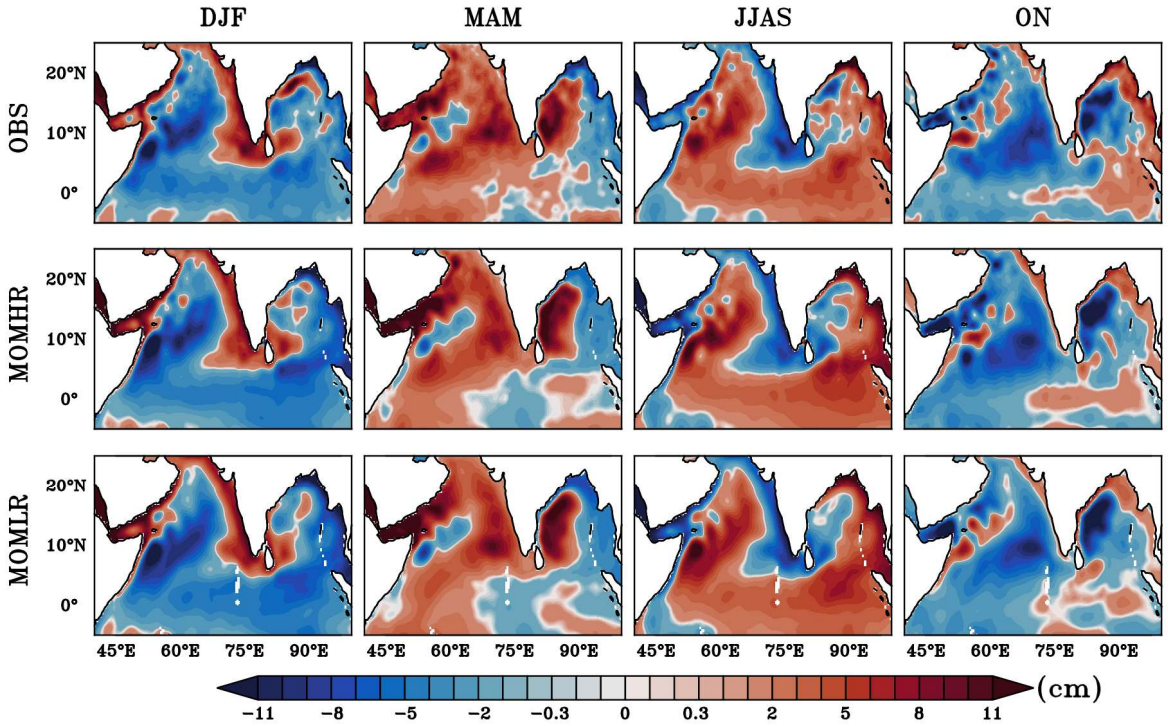

Figure 2: Seasonal mean sea level anomaly (SLA; cm) from altimeter (upper panel), MOMHR (middle panel) and MOMLR (lower panel) for the winter monsoon (DJF), pre monsoon (MAM), summer monsoon (JJAS) and post monsoon (ON).

3.1 Seasonal mean sea level anomaly

Figure 2 shows the comparison of seasonal mean sea level between altimeter and models. The seasons are defined based on the Indian monsoon system and are referred to as winter (December-February; DJF), spring (March-May; MAM), summer (June-September; JJAS) and fall (October-November; ON) (see, for example, Chatterjee et al. (2012) for more details about the oceanic temperature/salinity characteristics across theses different seasons).

Both the models could simulate the seasonal mean reasonably well within an error of about ± 3 cm in most part of the domain except at few locations where sea level signal is dominated by the eddy activities. During winter (DJF), eastern BoB experiences an upwelling signature all along the coast of Thailand/Myanmar mainly driven by upwelling favourable planetary waves forced by the equatorial winds (Iskander et al., 2009; Chen et al., 2016). Both the model could reproduce this feature well, except the fact that models tend to produce stronger upwelling signature with lower sea level by about~ 5 cm compared to the observation (Figure

3). At the same time, the west coast of India experiences sea level high induced by the downwelling coastal Kelvin waves forced in the BoB. On this occasion, models show higher sea level compared to the observations (Figure 3). This indicates that models are biased towards the lower vertical mode baroclinic waves which exhibited these stronger coastal signals along the eastern boundary of the BoB and the west coast of India. As the wind reverses during summer (JJAS), the models show positive bias in the eastern BoB and negative bias along the west coast of India. Note, however, that while both the models produce a very similar sea level bias in the seasonal cycle, the coastal signals are a bit stronger in the MOMLR than MOMHR which resulted in significantly higher bias in MOMLR. As the small scale, higher order, vertical modes turn significant close to the coast and or in the strong current regim, MOMLR likely aliases the small scale variability onto the larger scale owing to its coarse resolution and thereby produces stronger mesoscale signal than the observation in these regions. These anomalously stronger mean currents in MOMLR is more conspicuous along the eastern and northern boundary of the BoB, along the west coast of India and swift current system off Somalia coast associated with Great Whirl (Figure 2, 3). On the other hand, MOMHR can capture higher order vertical modes relatively well and thus compare better with the observation.

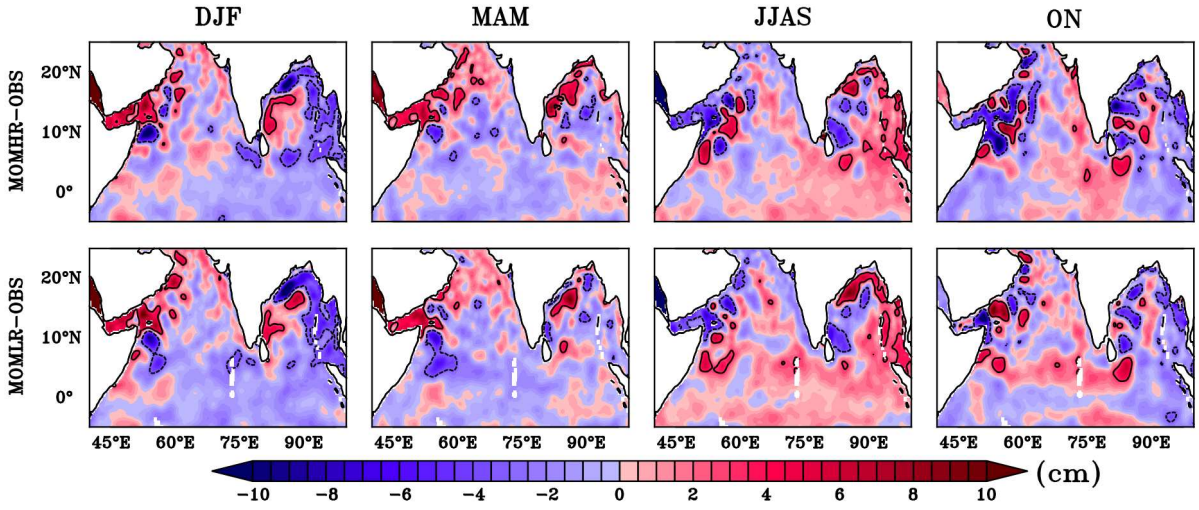

Figure 3: The bias of simulated seasonal mean SLA (cm) from MOMHR (upper) and MOMLR (bottom) for the different seasons.

3.2 Seasonal and mesoscale variability

The standard deviation of the altimeter suggests that variability of SLA is much stronger in the BoB compared to the AS (Figure 4). In the AS, variability hotspots are primarily limited to the Somali region which is known to be strongly driven by seasonally unstable eddies, the coast of Arabia owing to the coastal upwelling during summer and then to some extent west coast of India. On the other hand, the sea level variability is spread over the BoB with energy hotspots along the eastern and northern boundary of the BoB, western part of the BoB starting from the east coast of Srilanka to off Gopalpur of Orisha and the southern BoB in the interior. Both the models reproduce the spatial observed variability reasonably well with the fact that the magnitude of the variability simulated by the MOMLR is weak compared to the MOMHR and the observation (Figure 4). Simulated SLA variability in MOMHR is much closer to the observation. The major differences between the MOMLR and MOMHR are mostly confined to the regions where the nonlinearity of the system is important. For example, in the Somali region, altimeter and MOMHR show much stronger variability spread over a much broader area covering the entire latitudinal extent of the Somali coast with an eastward extent up to 65^{o}E-70^{o}E. In contrast, variability in MOMLR is mostly confined within the spatial extent of Great Whirl in the northern part of the coast and the energy decreases rapidly in the south. The eastward extension of this variability in MOMLR is also weak compared to the observation and MOMHR. Similarly, in the western BoB, a region is known for strong eddy activity (Mukherjee et al., 2019), MOMHR could reproduce observed variability quite well. Whereas, MOMLR show much weaker variability owing to the less active eddy generation in this region.

A comparison of the ratio of the variance with respect to observation indicates that MOMLR tends to severely underestimate the variability in most part of the Indian Ocean, particularly in the interior basin and in the western Arabian Sea and along the EICC regime (Figure S2). However, along the eastern and northern boundary of the BoB and along the west coast of

India, MOMLR produces much stronger variability than the MOMHR and the altimeter indicating possible aliasing of high-frequency variability into the larger scales in the coarser model as was also observed in mean seasonal sea level signals (Figure 3).

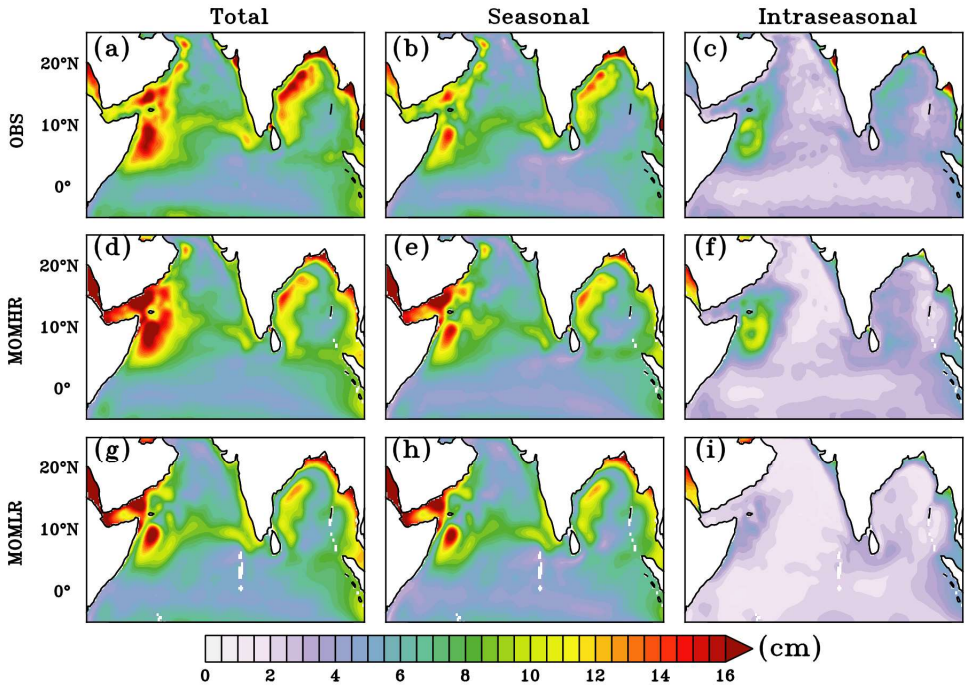

Figure 4: Standard deviation of (a) observed SLA (cm), (b) filtered for the seasonal time scale (100 days lowpass) and (c) filtered for the intraseasonal timescale (100 days highpass) from the altimeter. (d-f) is the same for MOMHR and (g-i) for the MOMLR.

In order to understand these differences, seasonal (more than 100 days period; Figure 4 b,e,h) and mesoscale (10-100 days period; Figure 4 c,f,i) variability are calculated separately. As expected, the seasonal scale dominates the variability in the Indian Ocean and comprise more than 90% variability in most part of the domain. The mesoscale variability is much weaker and limited to the well known active non-linear regions. Both the models simulate the seasonal variability well. Interestingly, in this timescale, MOMLR exhibits relatively stronger variability compared to the altimeter, particularly for the coastal current systems off the west coast of India and in the eastern boundary of the BoB. This agrees with the fact that the low frequency planetary coastally trapped waves are strongly excited in the coarser model as noted earlier resulting in a strong seasonal current along these regions. A similar strong variability is also seen in the core of the Great Whirl eddy in the Somali region owing to the

lateral movement of mean current associated with this eddy during the course of its life cycle which extends from May-November (Beal and Donohue, 2013; Chatterjee et al., 2019). On the contrary, for the mesoscale spectrum, MOMLR failed to produce the observed variability for the entire north IO. MOMHR, on the other hand, produces the magnitude and spatial extent of this mesoscale variability quite well. Note, however, that MOMHR shows weaker mesoscale variability compared to the observation in the western part of the BoB, a region known for stronger eddy activities associated with nonlinearity embedded within the westward propagating Rossby waves (Cheng et al., 2015; Mukherjee et al., 2019). But, in the Somali region, MOMHR shows higher variability compared to the altimeter and is driven by enhanced instabilities associated with the Somali current in the high resolution model. Both of these features are completely absent in the MOMLR indicating weaker nonlinearity driven mesoscale flows that spin-off from the mean seasonal current in the observation and the high resolution model.

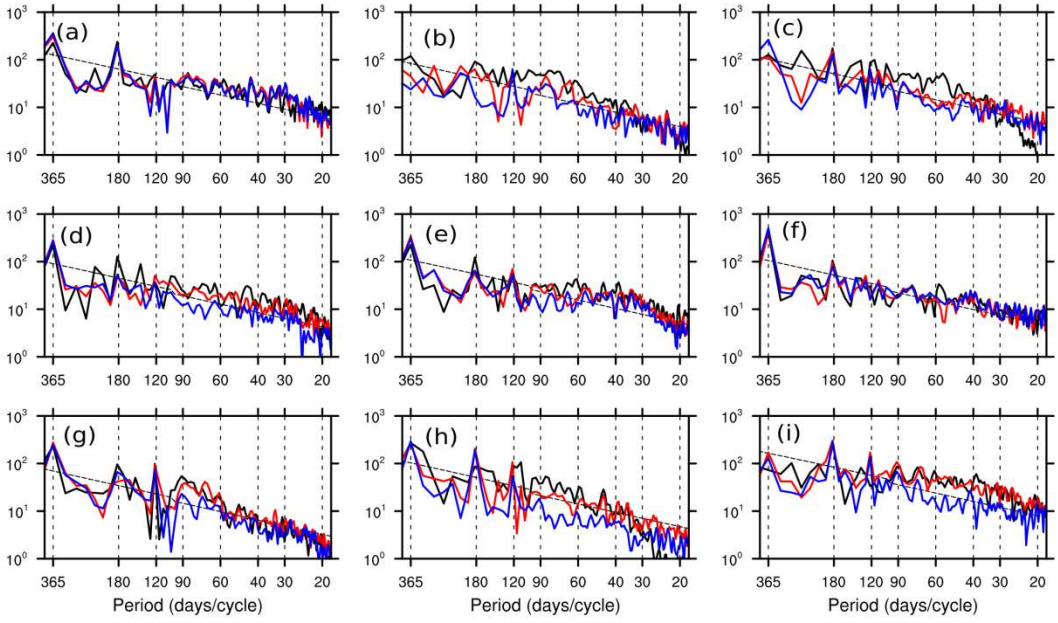

Figure 5: Comparison of power spectra of SLA between altimeter (black), MOMHR (red) and MOMLR (blue) at selected locations (see Figure 1) in the north Indian ocean.

Further, Figure 5 shows that spectral power across the frequency bands at a few selected coastal (a-g) and open ocean (h, i) locations to test the models' ability in reproducing

dominant spectral peaks. The best performance of the models is seen for the location off the coast of Thailand (Figure 5a) and Java (Figure 5e). Here, both the models could reproduce the observed spectral peaks across the spectral bands remarkably well. This supreme performance by both models at these locations is owing to the proximity of the equator and most importantly variability is driven dominantly by the equatorial forcing. As the equatorial responses are comprised mainly of the first two baroclinic modes (Schott and McCreary, 2001; Han et al., 2001; Chatterjee et al., 2017) and thereby, reproduced well by both the models. Model performance generally degrades away from the equatorial region, particularly for the MOMLR. Off Gopalpur (Figure 5c), in the northern part of the east coast of India, while both models could reproduce semiannual and annual cycle reasonably well, but failed completely for the intraseasonal band. Here, both the models exhibit weaker amplitude in 30-100 days band but show stronger amplitude for the high frequency band of 10-30 days. In fact, at all locations, models show higher energy at this high frequency band of 10-30 days period than the observation. This weaker energy in the altimeter for this high frequency band may be linked to its coarse sampling. A similar performance can be seen in the central BoB (Figure 5b) where both the models failed to produce the observed mesoscale variability. The inability of the models, despite an enhancement in the horizontal and vertical resolution in MOMHR, possibly indicates the importance of small scale atmospheric forcing in the Bay of Bengal which modulates such high frequency variability in the observation. The prescribed 0.25^{o} forcing fields do not resolve these scales well and therefore, likely underestimate energy in the intraseasonal spectrum which reflects in the underestimation of model simulations. Another possible source of error is the erroneous representations of the Andaman and Nicobar Islands in the models which shown to influence the radiation of the Rossby waves and associated embedded eddies from the eastern BoB. Chatterjee et al. (2017) demonstrated earlier that the misrepresentation of these island chains may result in large sea level anomaly blobs in the western part of the basin owing to the alteration in the phase of the radiated

Rossby waves. Comparison in the intraseasonal band improves at the southern latitude off the east coast of Sri Lanka. But, here unlike central and northern BoB, MOMHR could reproduce the observe variability remarkably well as the intraseasonal variability in this latitude band (Figure 4 e,f) driven mainly by reflected Rossby waves from the eastern boundary of the Bay of Bengal (Cheng et al., 2013) simulated accurately by the high resolution model. Here also mesoscale energy is relatively weak in the MOMLR as was observed in the rest of the BoB. The performance of the models improve significantly off Kochi (Figure 5f) owing to the greater influence of the equatorial forcing in the sea level variability at this location (Vialard et al., 2009; Suresh et al., 2013). In the western Arabian Sea (Figure 5h,i) a clear distinction in the performance between the models can be established. While both the models reproduce the observed seasonal variability well, for the mesoscale band MOMLR shows much weaker energy compared to the observation. Interestingly, MOMHR does a reasonably good job in reproducing the observed variability off the coast of Arabia and Somalia. This suggests that the high resolution model is necessary to simulate the observed intraseasonal variability of this region well. It further indicates that unlike BoB, where the mesoscale variability is driven by oceanic internal instabilities, high resolution model can provide a more realistic simulation than the coarser model. Moreover, similarly improved performance by the high resolution model is seen for the central Arabian Sea as well (Figure 5g). But here MOMLR also does well except for the 60-100 days band where it shows weaker amplitude as compared to the observation. This better simulation in the central Arabian Sea compared to the central BoB, despite both are at the same latitude, is likely owing to the fact that the Arabian Sea experiences relatively weaker small scale atmospheric forcing, weaker nonlinearities and the absence of any complex bathymetry like Andaman and Nicobar Islands in the BoB.

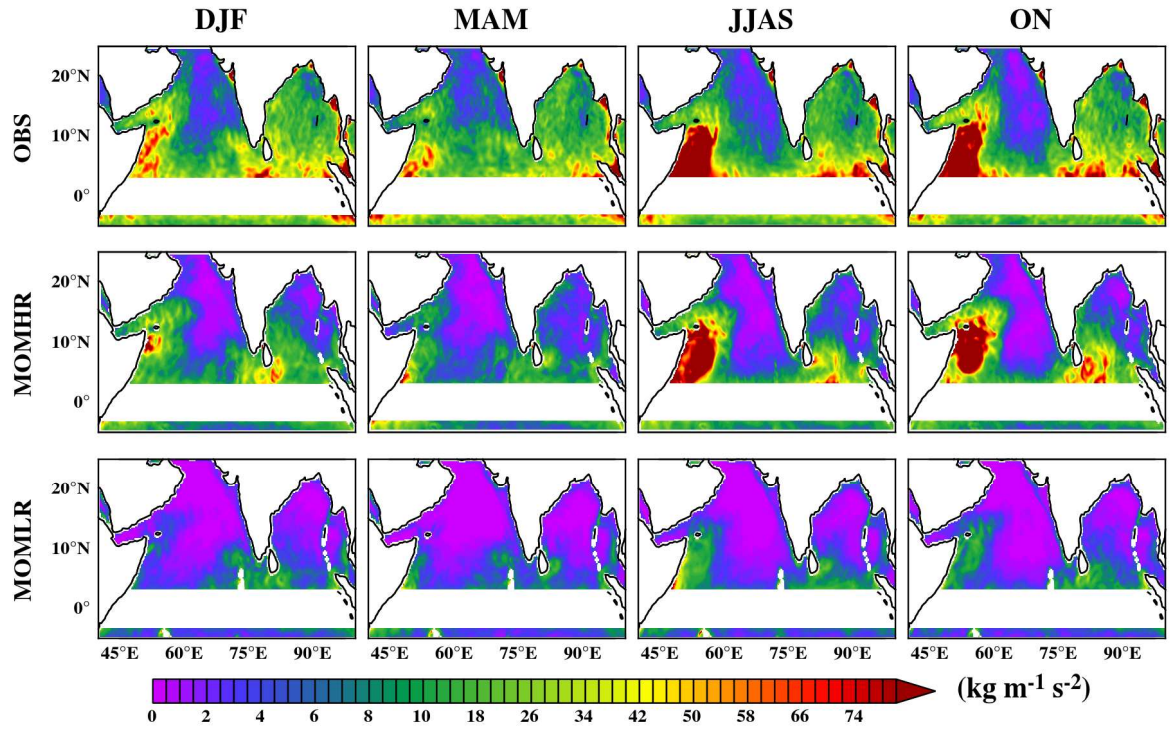

Figure 6: The seasonal geostrophic eddy kinetic energy (EKE) for the surface geostrophic fields for the observation (upper panel), MOMHR (middle panel) and MOMLR (lower panel).

3.3 Geostrphic vs. ageostrophic

The eddy kinetic energy (EKE) of the observed and model simulated surface geostrophic fields are calculated based on SLA from the respective datasets (Figure 6). As seen in the previous sections, the geostrophic EKE derived from MOMHR resembles well with the observation. The only notable difference is that MOMHR produces slightly weaker energy throughout the model domain which is particularly conspicuous for the BoB and in the north-central part of the Arabian Sea. On the other hand, MOMLR produces much weaker geostrophic current even in the strong current regimes like Somali current off the coast of Somalia and summer monsoon current southeast of Sri Lanka. The coastal currents (EICC and WICC) along the coast of India does not show up in these plots (across the datasets) due to averaging of opposite phases of the coastally trapped waves within a season.

In order to understand the contribution of ageostrphic component in the total EKE, Figure 7 shows the difference of the total EKE to the geostrphic fields, an estimate of the ageostrophic fields. Here, the total EKE for the observation is calculated based on daily surface currents

from Sikhakolli et al., (2013) and for the models, it is calculated based on simulated surface current fields from the respective model. A striking difference between MOMHR and MOMLR is that MOMHR shows an asymmetry in the Somali current regime during the summer monsoon with the positive contribution of ageostrphic surface currents in the north of the Somali coast and a negative contribution in the regime of Great Whirl return flow in the south. The observation also suggests that a similar process is active in this region albeit much scattered unlike in the high resolution model. The scatterness might have come owing to the use of two independent data sets (for sea level and current) for the calculation.

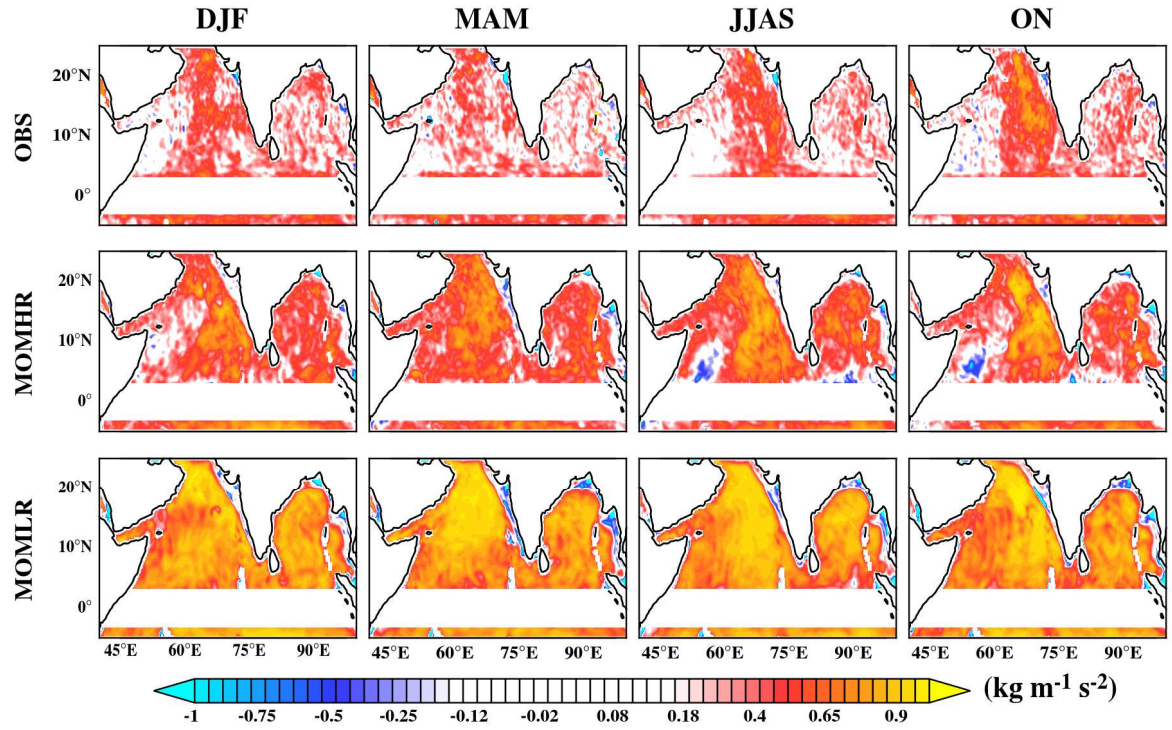

Figure 7: Ageostrophic eddy kinetic energy for the observation (upper panels), MOMHR (middle panels) and MOMLR (lower panels) for different seasons.

In contrast, MOMLR shows a unified positive contribution of ageostrphic field in this region. The negative contribution of the ageostrophic flow in the total EKE in the southern part of the Great whirl return flow regime is owing to the strong curvature in the strong current which can no more get balanced by the weaker Coriolis force in this latitude and thus driven by the gradient wind balance which is a balance between centripetal acceleration and the pressure gradient force (Douglass and Richman, 2015; Chassignet and Xu, 2017). Interestingly, in the

rest of the domain where the nonlinearity is much weak, MOMLR shows a much stronger ageostrophic contribution in the total EKE. This indicates that in the coarser model surface Ekman velocities are much stronger than the high resolution model. This is due to the fact that air-sea coupling is stronger for the lower order vertical modes (Shankar et al., 1996) which are preferentially get exited by the winds in MOMLR. Notably, while ageostrophic flow fields contribute about 20-30% of the total EKE for the MOMHR model in the open ocean, it reaches to 100% or more for most of the interior circulation in the MOMLR (Figure 7).

4. Summary

The influence of increasing horizontal and vertical resolution in an oceanic general circulation model is investigated in simulating the observed sea level anomaly. The sea level simulated by a coarser model of $1/4^{o}$ horizontal resolution with 40 vertical levels (MOMLR) is compared with the simulation from a much higher resolution $1/20^{o}$ with 50 vertical levels (MOMHR). Both the model faithfully simulates the seasonal patterns of sea level anomaly for the north Indian Ocean. However, MOMHR shows significant improvement in the simulation of variability and frequency spectra across the domain over MOMLR. Particularly, the coastal sea level variability along the coast of India, in the eastern boundary of the BoB and in the western AS is better represented in the MOMHR. For the mesoscale variability (intraseasonal time scale) sea level signal simulated reasonably well in MOMHR, whereas MOMLR failed to produce the observed variability in most part of the north Indian Ocean. Note, however, that both the models produce weaker magnitude for the mesoscale spectrum in central and northern BoB indicating possible physical mechanisms absence in both the models. An analysis of EKE show that EKE contributed by geostrophic circulation is reasonably captured by the MOMHR for the most part of the Indian Ocean except for the BoB and the central Arabian Sea where the geiostrophic velocities are relatively weaker than the velocities derived from the altimeter observation. On the other hand, geostrophic velocity fields are much weaker for the entire domain including the Somali region and south of Sri Lanka where the

mean currents are strongest in the Indian Ocean. Whereas, compared to the observation and MOMHR, MOMLR shows a much stronger ageostrophic contribution in the total EKE specifically in the open oceans. This dominant ageostrophic component in MOMLR is due to the excitation of stronger surface Ekman velocities driven by strong air-sea coupling for the lower order vertical modes which preferentially get generated by the winds in MOMLR. Nevertheless, ageostrophic component should become more important where fronts and strong meandering currents dominate as the velocity fields deviate from the geostrophic balance. The one such region in the Indian Ocean is the Great Whirl current regime where the positive contribution of ageostrphic surface currents in the north of the Somali coast and a negative contribution in the regime of Great Whirl return flow in the south is well captured by MOMHR. Our study concludes that the high resolution model helps in increasing the realism of the simulated seasonal signals and found to be necessary to simulate the observed mesoscale variability along the coasts and in the regime of strong current regime well.

Acknowledgement

We acknowledge the financial support provided by Indian National Centre for Ocean Information Services (INCOIS), Ministry of Earth Sciences(MoES), Govt. of India, to conduct this research. The first author is grateful to INCOIS, MoES for the Ph D fellowship, Kerala University of Fisheries and Ocean Studies(KUFOS) for providing the necessary facilities. This is INCOIS contribution number XXXX .

Conflict of Interest

The authors declare that the research was conducted in the absence of any commercial or financial relationships that could be construed as a potential conflict of interest.

Data Availability Statement

The Sea Level Anomalies (SLA) data from AVISO used in this study is openly available at https://www.aviso.oceanobs.com/fr/accueil/index.html and ocean surface current data from

MOSDAC, ISRO is downloaded from http://www.mosdac.gov.in. The model simulations are carried out on the supercomputer Mihir installed at National Centre for Medium Range Weather Forecasting (NCMRWF), Delhi and will be made available upon request.

Reference

Amol, P., Shankar, D., Aparna, S. G., Shenoi, S. S. C., Fernando, V., Shetye, S. R., Mukherjee, A., Agarvadekar, Y., Khalap, S. and Satelkar, N. P. 2012. Observational evidence from direct current measurements for propagation of remotely forced waves on the shelf off the west coast of India. *Journal of Geophysical Research: Oceans*, *117*(C5). https://doi.org/10.1029/2011JC007606

Beal, L. M., and Donohue, K. A. 2013. The Great Whirl: Observations of its seasonal development and interannual variability. *Journal of Geophysical Research: Oceans*, *118*(1), 1-13. https://doi.org/10.1029/2012JC008198

Biri, S., Serra, N., Scharffenberg, M. G., and Stammer, D. 2016. Atlantic sea surface height and velocity spectra inferred from satellite altimetry and a hierarchy of numerical simulations. *Journal of Geophysical Research: Oceans*, *121*(6), 4157-4177. https://doi.org/10.1002/2015JC011503

Brunet, G., Shapiro, M., Hoskins, B., Moncrieff, M., Dole, R., Kiladis, G. N., Kirtman, Ben., Lorenc, A., Mills, B., Morss, R., Polavarapu, S., Rogers, D., Schaake, J. and Shukla, J. 2010. Collaboration of the weather and climate communities to advance subseasonal-to-seasonal prediction. *Bulletin of the American Meteorological Society*, *91*(10), 1397-1406. https://doi.org/10.1175/2010BAMS3013.1

Chassignet, E. P., and Xu, X. 2017. Impact of horizontal resolution (1/12 to 1/50) on Gulf Stream separation, penetration, and variability. *Journal of Physical Oceanography*, *47*(8), 1999-2021. https://doi.org/10.1175/JPO-D-17-0031.1

Chatterjee, A., Shankar, D., Shenoi, S. S. C., Reddy, G. V., Michael, G. S., Ravichandran, M., Gopalkrishna, V.V., Rao, E.R., Bhaskar, T.U. and Sanjeevan, V. N. 2012. A new atlas of temperature and salinity for the North Indian Ocean. *Journal of Earth System Science*, *121*(3), 559-593. https://doi.org/10.1007/s12040-012-0191-9

Chatterjee, A., Shankar, D., McCreary Jr, J. P., and Vinayachandran, P. N. 2013. Yanai waves in the western equatorial Indian Ocean. *Journal of Geophysical Research: Oceans*, *118*(3), 1556-1570. https://doi.org/10.1002/jgrc.20121

Chatterjee, A., Shankar, D., McCreary, J. P., Vinayachandran, P. N., and Mukherjee, A. 2017. Dynamics of A ndaman S ea circulation and its role in connecting the equatorial I ndian O cean to the B ay of B engal. *Journal of Geophysical Research: Oceans*, *122*(4), 3200-3218. https://doi.org/10.1002/2016JC012300

Chatterjee, A., Kumar, B. P., Prakash, S., and Singh, P. 2019. Annihilation of the Somali upwelling system during summer monsoon. *Scientific reports*, *9*(1), 1-14. https://doi.org/10.1038/s41598-019-44099-1

Chaudhuri, A., Shankar, D., Aparna, S. G., Amol, P., Fernando, V., Kankonkar, A., Michael, G.S., Satelkar, N.P., Khalap, S.T., Tari, A.P. and Gaonkar, M.G., Ghatkar, S. and Khedekar, R. R. 2020. Observed variability of the West India Coastal Current on the continental slope from 2009–2018. *Journal of Earth System Science*, *129*(1), 1-23. https://doi.org/10.1007/s12040-019-1322-3

Chen, G., Han, W., Li, Y., and Wang, D. 2016. Interannual variability of equatorial eastern Indian Ocean upwelling: Local versus remote forcing. *Journal of Physical Oceanography*, *46*(3), 789-807. https://doi.org/10.1175/JPO-D-15-0117.1

Cheng, X., Xie, S. P., McCreary, J. P., Qi, Y., and Du, Y. 2013. Intraseasonal variability of sea surface height in the Bay of Bengal. *Journal of Geophysical Research: Oceans*, *118*(2), 816-830. https://doi.org/10.1002/jgrc.20075

Douglass, E. M., and Richman, J. G. 2015. Analysis of ageostrophy in strong surface eddies in the A tlantic O cean. *Journal of Geophysical Research: Oceans*, *120*(3), 1490-1507. https://doi.org/10.1002/2014JC010350

Ducet, N., Le Traon, P. Y., and Reverdin, G. 2000. Global high-resolution mapping of ocean circulation from TOPEX/Poseidon and ERS-1 and-2. *Journal of Geophysical Research: Oceans*, *105*(C8), 19477-19498. https://doi.org/10.1029/2000JC900063

Francis, P. A., Jithin, A. K., Effy, J. B., Chatterjee, A., Chakraborty, K., Paul, A., Balaji, B., Shenoy, S.S.C., Biswamoy, P., Mukherjee, A., Singh, P., Deepsankar, B., Siva Reddy, S., Vinayachandran, P.N., Girish Kumar., M.S., Udaya Bhaskar, T.V.S., Ravichandra, M., Unnikrishnan, A.S., Shankar, D., Prakash, A., Aparna, S.G., Harikumar, R., Kaviyazhahu, K., Suprit, K., Shesu, R.V., Kiran Kumar, N., Srinivasa Rao, N., Annapurnaiah, K., Venkatesan, R., Rao, A.S., Rajagopal E.N., Prasad, V.S., Gupta, M.D., Balakrishnan Nair, T.M., Rao, E.P.R., and Satyanarayana, B. V. 2020. High-resolution operational ocean forecast and reanalysis system for the Indian ocean. *Bulletin of the American Meteorological Society*, *101*(8), E1340-E1356. https://doi.org/10.1175/BAMS-D-19-0083.1

Francis, P. A., Jithin, A. K., Chatterjee, A., Mukherjee, A., Shankar, D., Vinayachandran, P. N., and Ramakrishna, S. S. V. S. 2020. Structure and dynamics of undercurrents in the western boundary current of the Bay of Bengal. *Ocean Dynamics*, *70*(3), 387-404. https://doi.org/10.1007/s10236-019-01340-9

Ge, X., Wang, W., Kumar, A., and Zhang, Y. 2017. Importance of the vertical resolution in simulating SST diurnal and intraseasonal variability in an oceanic general circulation model. *Journal of Climate*, *30*(11), 3963-3978. https://doi.org/10.1175/JCLI-D-16-0689.1

Griffies, S. M., Winton, M., Anderson, W. G., Benson, R., Delworth, T. L., Dufour, C. O., Dunne, J.P., Goddard, P., Morrison, A.K., Rosati, A. and Wittenberg, A.T., Yin, J., and Zhang, R. 2015. Impacts on ocean heat from transient mesoscale eddies in a hierarchy of

climate models. *Journal of Climate*, *28*(3), 952-977. https://doi.org/10.1175/JCLI-D-14-00353.1

Griffies, S. M. 2012. Elements of the modular ocean model (MOM). *GFDL Ocean Group Tech. Rep*, *7*(620), 47.

Guo, Y., Li, Y., Wang, F., Wei, Y., and Xia, Q. 2020. Importance of resolving mesoscale eddies in the model simulation of Ningaloo Niño. *Geophysical Research Letters*, *47*(14), e2020GL087998. https://doi.org/10.1029/2020GL087998

Hallberg, R. 2013. Using a resolution function to regulate parameterizations of oceanic mesoscale eddy effects. *Ocean Modelling*, *72*, 92-103. https://doi.org/10.1016/j.ocemod.2013.08.007

Han, W., Lawrence, D. M., and Webster, P. J. 2001. Dynamical response of equatorial Indian Ocean to intraseasonal winds: Zonal flow. *Geophysical Research Letters*, *28*(22), 4215-4218. https://doi.org/10.1029/2001GL013701

Hewitt, H. T., Bell, M. J., Chassignet, E. P., Czaja, A., Ferreira, D., Griffies, S. M., Hyder, P., McClean, J.L., New, A.L. and Roberts, M. J. 2017. Will high-resolution global ocean models benefit coupled predictions on short-range to climate timescales?. *Ocean Modelling*, *120*, 120-136. https://doi.org/10.1016/j.ocemod.2017.11.002

Hewitt, H. T., Roberts, M., Mathiot, P., Biastoch, A., Blockley, E., Chassignet, E. P., Fox-Kemper, B., Hyder, P., Marshall, D.P., Popova, E., Treguier, A.M., Zanna, L., Yool, A., Yu, Y., Beadling, R., Bell, M., Kuhlbrodt, T., Arsouze, T., Bellicci, A., Castruccio, F., Gan, B., Putrasahan, D., Roberts, C. D., Roekel, L.V., and Zhang, Q. 2020. Resolving and parameterising the ocean mesoscale in earth system models. *Current Climate Change Reports*, 1-16. https://doi.org/10.1007/s40641-020-00164-w

Hurlburt, H. E., and Hogan, P. J. 2000. Impact of 1/8 to 1/64 resolution on Gulf Stream model–data comparisons in basin-scale subtropical Atlantic Ocean models. *Dynamics of Atmospheres and Oceans*, *32*(3-4), 283-329. https://doi.org/10.1016/S0377-0265(00)00050-6

Hurrell, J., Meehl, G. A., Bader, D., Delworth, T. L., Kirtman, B., and Wielicki, B. 2009. A unified modeling approach to climate system prediction. *Bulletin of the American Meteorological Society*, *90*(12), 1819-1832. https://doi.org/10.1175/2009BAMS2752.1

Iskandar, I., Masumoto, Y., and Mizuno, K. 2009. Subsurface equatorial zonal current in the eastern Indian Ocean. *Journal of Geophysical Research: Oceans*, *114*(C6). https://doi.org/10.1029/2008JC005188

Jia, Y., Richards, K. J., and Annamalai, H. 2021. The impact of vertical resolution in reducing biases in sea surface temperature in a tropical Pacific Ocean model. *Ocean Modelling*, *157*, 101722. https://doi.org/10.1016/j.ocemod.2020.101722

Kalnay, E., Kanamitsu, M., Kistler, R., Collins, W., Deaven, D., Gandin, L., Iredell, M., Saha, S., White, G., Woollen, J., Zhu, Y., Leetmaa, A., Reynolds, B., Chelliah, M., Ebisuzaki, W., Higgins, W., Janowiak, J., Mo, K.C., Ropelewski, C., Wang, J., Jenne, R., and Joseph, D.

1996. The NCEP/NCAR 40-year reanalysis project. *Bulletin of the American meteorological Society*, *77*(3),437-472.https://doi.org/10.1175/1520-0477(1996)077<0437:TNYRP>2.0.CO;2

Kirtman, B. P., Bitz, C., Bryan, F., Collins, W., Dennis, J., Hearn, N., Kinter, J.L., Loft, R., Rousset, C., Siqueira, L., Stan, C., Tomas, R. and Vertenstein, M. 2012. Impact of ocean model resolution on CCSM climate simulations. *Climate dynamics*, *39*(6), 1303-1328. https://doi.org/10.1007/s00382-012-1500-3

Kurian, J., and Vinayachandran, P. N. 2006. Formation mechanisms of temperature inversions in the southeastern Arabian Sea. *Geophysical research letters*, *33*(17). https://doi.org/10.1029/2006GL027280

Lakshmi, R. S., Chatterjee, A., Prakash, S., and Mathew, T. 2020. Biophysical interactions in driving the summer monsoon chlorophyll bloom off the Somalia coast. *Journal of Geophysical Research: Oceans*, *125*(3), e2019JC015549. https://doi.org/10.1029/2019JC015549

Large, W. G., McWilliams, J. C., and Doney, S. C. 1994. Oceanic vertical mixing: A review and a model with a nonlocal boundary layer parameterization. *Reviews of geophysics*, *32*(4), 363-403. https://doi.org/10.1029/94RG01872

Lu, Y., Li, J., Lei, J., and Hannah, C. 2017. Impacts of model resolution on simulation of meso-scale eddies in the Northeast Pacific Ocean. *Satellite Oceanography and Meteorology*, 2(2): 328. http://dx.doi.org/10.18063/SOM.v2i2.328.

McCreary Jr, J. P., Kundu, P. K., and Molinari, R. L. 1993. A numerical investigation of dynamics, thermodynamics and mixed-layer processes in the Indian Ocean. *Progress in Oceanography*, *31*(3), 181-244. https://doi.org/10.1016/0079-6611(93)90002-U

Mukherjee, A., Shankar, D., Chatterjee, A., and Vinayachandran, P. N. 2018. Numerical simulation of the observed near-surface East India Coastal Current on the continental slope. *Climate Dynamics*, *50*(11), 3949-3980. https://doi.org/10.1007/s00382-017-3856-x

Mukherjee, A., Chatterjee, A., and Francis, P. A. 2019. Role of Andaman and Nicobar Islands in eddy formation along western boundary of the Bay of Bengal. *Scientific reports*, *9*(1), 1-10. https://doi.org/10.1038/s41598-019-46542-9

Mukhopadhyay, S., Shankar, D., Aparna, S. G., Mukherjee, A., Fernando, V., Kankonkar, A., Khalap, S., Satelkar, N.P., Gaonkar, M.G., Tari, A.P., Khedekar, R.R. and Ghatkar, S. 2020. Observed variability of the East India Coastal Current on the continental slope during 2009–2018. *Journal of Earth System Science*, *129*(1), 1-22. https://doi.org/10.1007/s12040-020-1346-8

Paul, B., Baduru, B., Paul, A., Francis, P. A., and Shetye, S. R. 2021. Absence of the annual cycle in shelf current inshore of the East Indian Coastal Current. *Continental Shelf Research*, *215*, 104355. https://doi.org/10.1016/j.csr.2021.104355

Penduff, T., Juza, M., Brodeau, L., Smith, G. C., Barnier, B., Molines, J. M., Treguier, A.M. and Madec, G. 2010. Impact of global ocean model resolution on sea-level variability with

emphasis on interannual time scales. *Ocean Science*, *6*(1), 269-284. https://doi.org/10.5194/os-6-269-2010

Phillips, H. E., Tandon, A., Furue, R., Hood, R., Ummenhofer, C., Benthuysen, J., Menezes, V., Hu, S., Webber, B., Sanchez-Franks, A., Cherian, D., Shroyer, E., Feng, M., Wijeskera, H., Chatterjee, A., Yu, L., Hermes, J., Murtugudde, R., Tozuka, T., Su, D., Singh, A., Centurioni, L., and Wiggert, J. 2021. Progress in understanding of Indian Ocean circulation, variability, air-sea exchange and impacts on biogeochemistry. *Ocean Science Discussions*, 1-109. https://doi.org/10.5194/os-2021-1

Prerna, S., Chatterjee, A., Mukherjee, A., Ravichandran, M., and Shenoi, S. S. C. 2019. Wyrtki Jets: Role of intraseasonal forcing. *Journal of Earth System Science*, *128*(1), 21. https://doi.org/10.1007/s12040-018-1042-0

Roberts, M. J., Banks, H., Gedney, N., Gregory, J., Hill, R., Mullerworth, S., Pardaens, A., Rickard, G., Thorpe, R. and Wood, R. 2004. Impact of an eddy-permitting ocean resolution on control and climate change simulations with a global coupled GCM. *Journal of Climate*, *17*(1), 3-20. https://doi.org/10.1175/1520-0442(2004)017<0003:IOAEOR>2.0.CO;2

Roberts, M. J., Clayton, A., Demory, M. E., Donners, J., Vidale, P. L., Norton, W., Shaffrey, L., Stevens, D.P., Stevens, I., Wood, R.A. and Slingo, J. 2009. Impact of resolution on the tropical Pacific circulation in a matrix of coupled models. *Journal of Climate*, *22*(10), 2541-2556. https://doi.org/10.1175/2008JCLI2537.1

Sandery, P. A., and Sakov, P. 2017. Ocean forecasting of mesoscale features can deteriorate by increasing model resolution towards the submesoscale. *Nature Communications,8,* 1566. https://doi.org/10.1038/s41467-017-01595-0.

Schott, F. A., and McCreary Jr, J. P. 2001. The monsoon circulation of the Indian Ocean. *Progress in Oceanography*, *51*(1), 1-123. https://doi.org/10.1016/S0079-6611(01)00083-0

Schott, F. A., Xie, S. P., and McCreary Jr, J. P. 2009. Indian Ocean circulation and climate variability. *Reviews of Geophysics*, *47*(1). https://doi.org/10.1029/2007RG000245

Shankar, D., McCreary, J. P., Han, W., and Shetye, S. R. 1996. Dynamics of the East India Coastal Current: 1. Analytic solutions forced by interior Ekman pumping and local alongshore winds. *Journal of Geophysical Research: Oceans*, *101*(C6), 13975-13991. https://doi.org/10.1029/96JC00559

Shankar, D., Vinayachandran, P. N., and Unnikrishnan, A. S. 2002. The monsoon currents in the north Indian Ocean. *Progress in oceanography*, *52*(1), 63-120. https://doi.org/10.1016/S0079-6611(02)00024-1

Shankar, D., Remya, R., Vinayachandran, P. N., Chatterjee, A., and Behera, A. 2016. Inhibition of mixed-layer deepening during winter in the northeastern Arabian Sea by the West India Coastal Current. *Climate dynamics*, *47*(3), 1049-1072. https://doi.org/10.1007/s00382-015-2888-3

Shukla, J., Hagedorn, R., Hoskins, B., Kinter, J., Marotzke, J., Miller, M., Palmer, T.N and Slingo, J. 2009. Revolution in climate prediction is both necessary and possible: A declaration at the World Modelling Summit for Climate Prediction. *Bulletin of the American Meteorological Society*, *90*(2), 175-178. https://www.jstor.org/stable/26220947

Sikhakolli, R., Sharma, R., Kumar, R., Gohil, B. S., Sarkar, A., Prasad, K. V. S. R., and Basu, S. 2013. Improved determination of Indian Ocean surface currents using satellite data. *Remote sensing letters*, *4*(4), 335-343. https://doi.org/10.1080/2150704X.2012.730643

Sindhu, B., Suresh, I., Unnikrishnan, A. S., Bhatkar, N. V., Neetu, S., and Michael, G. S. 2007. Improved bathymetric datasets for the shallow water regions in the Indian Ocean. *Journal of Earth System Science*, *116*(3), 261-274. https://doi.org/10.1007/s12040-007-0025-3

Smith, R. D., Maltrud, M. E., Bryan, F. O., and Hecht, M. W. 2000. Numerical simulation of the North Atlantic Ocean at 1/10. *Journal of Physical oceanography*, *30*(7), 1532-1561. https://doi.org/10.1175/1520-0485(2000)030<1532:NSOTNA>2.0.CO;2

Stewart, K. D., Hogg, A. M., Griffies, S. M., Heerdegen, A. P., Ward, M. L., Spence, P., and England, M. H. 2017. Vertical resolution of baroclinic modes in global ocean models. *Ocean Modelling*, *113*, 50-65. https://doi.org/10.1016/j.ocemod.2017.03.012

Vialard, J., Shenoi, S. S. C., McCreary, J. P., Shankar, D., Durand, F., Fernando, V., and Shetye, S. R. 2009. Intraseasonal response of the northern Indian Ocean coastal waveguide to the Madden-Julian Oscillation. *Geophysical Research Letters*, *36*(14). https://doi.org/10.1029/2009GL038450